The Relationship of the Redox Potentials of Thioredoxin and Thioredoxin Reductase from *Drosophila melanogaster* to the Enzymatic Mechanism: Reduced Thioredoxin Is the Reductant of Glutathione in *Drosophila*†

Zhiyong Cheng,‡ L. David Arscott, David P. Ballou, and Charles H. Williams, Jr.*

Department of Biological Chemistry, University of Michigan Medical School, Ann Arbor, Michigan 48109-0606

Received March 5, 2007; Revised Manuscript Received April 25, 2007

ABSTRACT: Thioredoxin reductase from *Drosophila melanogaster* (DmTrxR) catalyzes the reversible transfer of reducing equivalents between NADPH and thioredoxin (Trx), a small protein that is involved in a wide variety of biological redox processes. The catalysis involves three essential redox states of the enzyme: the oxidized form of DmTrxR (E_{ox}), the 2-electron-reduced forms (EH_2), and the 4-electron-reduced forms (EH_4). In the present work, the macroscopic redox potentials of E_{ox}/EH_2 and EH_2/EH_4 couples were determined to be -272 ± 5 mV for $E_m(E_{ox}/EH_2)$ and -298 ± 11 mV for $E_m(EH_2/EH_4)$ on the basis of redox equilibria between DmTrxR and NADH. The value for $E_m(EH_2/EH_4)$ obtained from the steady-state kinetics of the TrxR-catalyzed reaction between NADPH and *D. melanogaster* Trx-2 (DmTrx-2) was reasonably consistent with that based on redox equilibria. The redox potential of the Trx-$(S)_2$/Trx-$(SH)_2$ couple from *D. melanogaster* Trx-2 (DmTrx-2) was calculated to be -275.4 ± 0.3 mV by using the Nernst equation and the K_{eq} for the equilibrium of the reaction involving NADP/NADPH and Trx-$(S)_2$/Trx-$(SH)_2$. For the accurate determination of the K_{eq}, an improved protocol has been developed to minimize errors that can be introduced by using starting concentrations far from equilibrium of the TrxR-catalyzed reaction between NADPH and Trx. This improved approach gives an E_m of -284.2 ± 1.0 mV for *Escherichia coli* Trx and -271.9 ± 0.4 mV for *Plasmodium falciparum* Trx, which agree well with published values (-283 or -285 mV and -270 mV, respectively). The redox potentials determined herein provide further direct evidence for the proposed catalytic mechanism of DmTrxR, and cast new light on the essential role of the DmTrx system in cycling GSSG/GSH and maintaining the intracellular redox homeostasis in *D. melanogaster* where glutathione reductase is absent.

Thioredoxin reductases (TrxR[1]) belong to the superfamily of homodimeric FAD-disulfide oxidoreductases that catalyze the transfer of electrons between pyridine nucleotides and disulfide/dithiol compounds using an FAD cofactor and one or more redox active disulfides (*1*). This family, which includes glutathione reductase, plays essential roles in maintaining intracellular redox homeostasis and in protecting organisms from oxidative damage. Reduced thioredoxin, Trx-$(SH)_2$, produced in the reaction catalyzed by TrxR, participates in a number of processes of physiological significance, such as antioxidant defense, DNA synthesis/repair, redox-signaling regulation, and apoptosis (*4*, *5*). In *Drosophila melanogaster*, which does not have a genuine glutathione reductase, the Trx-system is especially important because, in addition to its normal roles, it recycles GSSG (*2*, *3*).

A model for the catalytic mechanism of TrxR from *D. melanogaster* (DmTrxR) (Scheme 1) shows the path of electron flow from NADPH to FAD, from the reduced flavin to the N-terminal disulfide (Cys^{57}-Cys^{62}) adjacent to the flavin, from the nascent N-terminal dithiol pair of one subunit to the C-terminal redox pair of the neighboring subunit ($Cys^{489'}$-$Cys^{490'}$), and finally to the bound substrate, thioredoxin (Trx-$(S)_2$) (*6*−*8*). During catalysis, the enzyme cycles between 2-electron and 4-electron-reduced forms, which are indicated in Scheme 1 as EH_2 and EH_4, respectively. DmTrxR is reduced by 1 equiv NADPH to 2-electron-reduced forms (EH_2) prior to catalysis, and is further reduced by a second equivalent of NADPH to form 4-electron-reduced forms (EH_4) during catalysis. The catalytic cycle in Scheme 1 shows where the oxidizing substrate, thioredoxin-2 from *D. melanogaster* (DmTrx-2), a small protein of M_r 12,000 having one redox active disulfide−dithiol in the highly conserved -WCGPC- motif, interacts with TrxR (*9*). The N-terminal active thiol of DmTrx-2 is known to be

† This work was supported by grants from the National Institute of General Medical Science, GM21444 (to C.H.W.) and GM11106 (to D.P.B.).

* Correspondence should be addressed to this author. E-mail: chaswill@umich.edu. Phone: (734) 647-6989. Fax: (734) 763-4581.

‡ Present address: Howard Hughes Medical Institute, Department of Biological Chemistry and Molecular Pharmacology, Harvard University Medical School, Boston, MA 02115.

[1] Abbreviations: A_{nnn}, absorbance at nnn nm; Trx, thioredoxin; TrxR, thioredoxin reductase; DmTrxR, thioredoxin reductase from *Drosophila melanogaster*; DmTrx-2, *Drosophila melanogaster* thioredoxin-2; Ec-Trx, thioredoxin from *E. coli*; PfTrx, thioredoxin from *Plasmodium falciparum*; E_{ox}, oxidized TrxR; EH_2, the two-electron-reduced form of TrxR; EH_4, the four-electron-reduced form of TrxR; Trx-$(S)_2$, oxidized thioredoxin; Trx-$(SH)_2$, reduced thioredoxin; CTC, charge-transfer complex; E_m, the midpoint redox potential; E_h, the redox potential of the redox equilibrium systems; K_{eq}, equilibrium constant; GSH, glutathione; GSSG; glutathione disulfide; THP, tris(hydroxypropyl)phosphine.

10.1021/bi700442r CCC: $37.00
Published on Web 06/06/2007

Scheme 1: A Schematic Diagram of the Catalytic Cycle of DmTrxR and Its Participation in GSSG Recycling[a]

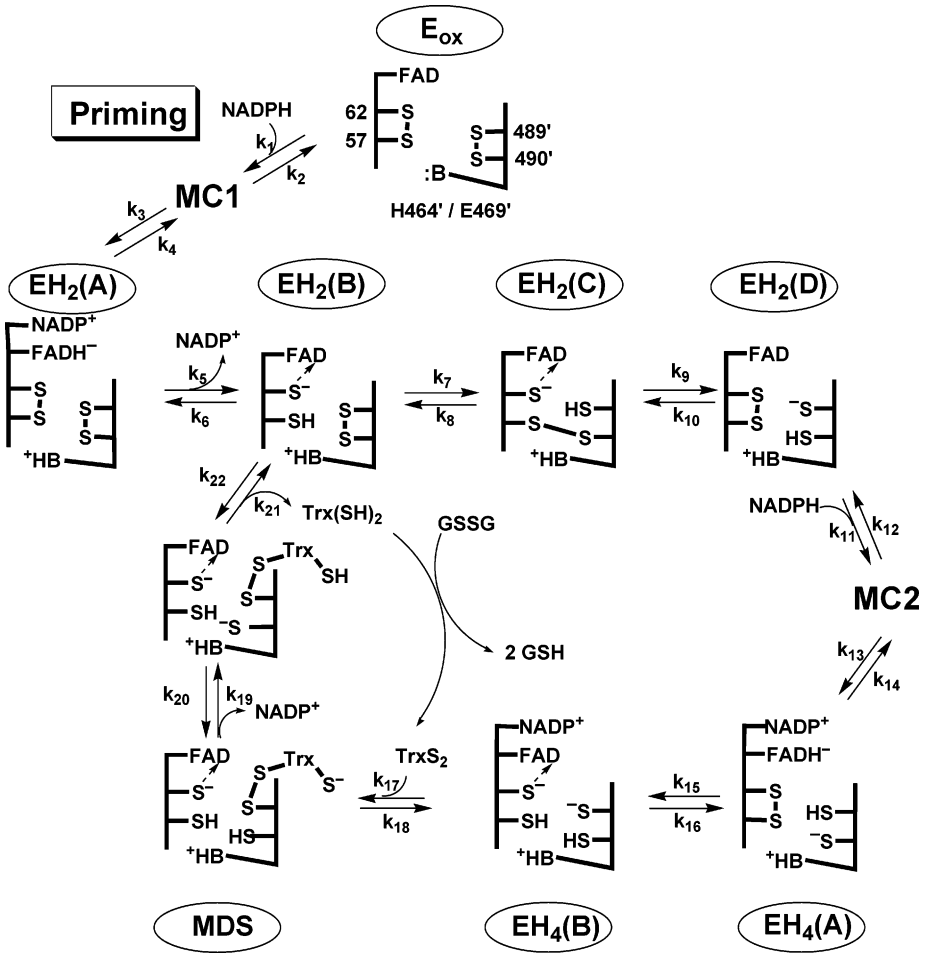

[a] MC, Michaelis complex. Activation of the enzyme by NADPH precedes catalysis (steps 1, 3, and 5).

exposed to solvent, and it can carry out a nucleophilic attack on disulfide substrates such as GSSG, ribonucleotide reductase, and methionine sulfoxide reductase (*4*, *5*, *10*).

DmTrxR-mediated catalysis, in essence, is the electron transfer process from NADPH to DmTrx-2, and the change in Gibbs free energy (ΔG) for each of the redox reactions in this process is highly dependent on the redox potential difference (ΔE_m) between the related redox couples ($\Delta G = -nF\Delta E_m$, where n is the number of electrons, and F is Faraday constant). Knowledge of the driving forces of electron transfer (ΔE_m) is important to our understanding of the catalytic mechanism of DmTrxR and its essential role in redox regulation/homeostasis in *D. melanogaster*. In the present work, we have measured the redox potentials of DmTrxR by redox titrations and steady-state kinetics method. An improved approach was developed to determine the equilibrium constant (K_{eq}) for the reactions between NADPH and DmTrx-2, where an important achievement was made to minimize the errors that can be introduced by traditional methods. Redox potentials of DmTrx-2 were calculated from the K_{eq} value using the Nernst equation. The redox potentials of thioredoxins from *Escherichia coli* and *Plasmodium falciparum* were determined by this improved approach and showed excellent agreement with the published values. The reactivity of GSSG with the Trx system, which includes thioredoxin reductase, thioredoxin, and NADPH, is discussed on the basis of the redox potentials determined here and the structural information available in literature.

MATERIALS AND METHODS

Chemicals. Ni-NTA agarose for purification of His-tagged proteins was from QIAGEN. NADPH, NADP, NADH, Sephadex G-25 resin, Ellman's reagent (5,5′-dithio-bis(2-nitrobenzoic acid)), and sodium borohydride ($NaBH_4$) were supplied by Sigma-Aldrich. Tris(hydroxypropyl)phosphine (THP) was purchased from Calbiochem. All other chemicals and reagents were from Fisher Scientific unless stated.

Preparation of His-Tagged TrxR and Trx. His-tagged DmTrxR (pQE-30/dmtrxr) and DmTrx-2 (pQE-30/dmtrx-2) were overexpressed in *E. coli* NovaBlue (Novagen, Inc.) as described previously (*6*, *9*). Trx and TrxR from *E. coli* (EcTrx and EcTrxR) and from *P. falciparum* (PfTrx and PfTrxR) were expressed and purified as previously described (*13*, *14*). SDS−PAGE (15% gel) showed single bands at the expected sizes of approximately 12 kDa for Trx and 55 kDa for TrxR. Thioredoxins were reduced as described by Aslund et al. (*15*, *16*) but using tris(hydroxypropyl)phosphine (THP) rather than dithiothreitol because it is more effective in reducing protein disulfide bonds (*17*). Ellman's reagent was used to check the quality of reduced proteins (*6*). Buffers were degassed and purged with argon and used for generation of reduced proteins, redox titrations, and steady-state kinetics studies.

Molar Extinction Coefficient. To enable accurate assays of the concentration of DmTrx-2, we determined its extinction coefficient at 278 nm where it shows maximum absorbance (*18*, *19*). Briefly, six aliquots were taken from a purified DmTrx-2 sample. The absorbance values at 278 nm (A_{278}) of three of the samples were measured, giving an average A_{278} of 0.381. The other three samples were submitted for amino acid analysis (*20*, *21*), and an average concentration of 52.05 μM was calculated based on the molecular weight of 13 kDa (*9*). On the basis of these measurements, the extinction coefficient of DmTrx-2 was calculated to be 7320 M^{-1} cm^{-1}; a value of 7879 M^{-1} cm^{-1} was calculated using the individual extinction coefficients of the spectrally active amino acids (*18*, *22*, *23*), and this value is in reasonable agreement with the experimentally determined value. The concentrations of *P. falciparum* Trx and *E. coli* Trx were determined from their absorbance at 280 nm using extinction coefficients of 11,700 M^{-1} cm^{-1} (*13*) and 13,700 M^{-1} cm^{-1} (*21*), respectively. Since reduction of thioredoxins by $NaBH_4$ (*6*) did not lead to significant changes in the absorbance at 280 nm, the concentration of reduced thioredoxin was determined using the extinction coefficient of the corresponding oxidized thioredoxin; these concentrations were further confirmed using Ellman's reagent (*6*). The concentrations of DmTrxR, PfTrxR, and EcTrxR were measured at 462 nm (ϵ_{462} = 11,900 M^{-1} cm^{-1}) (*6*), 460 nm (ϵ_{460} = 11,300 M^{-1} cm^{-1}) (*24*), and 456 nm (ϵ_{456}= 11,300 M^{-1} cm^{-1}) (*25*), respectively.

The concentration of NADPH was calculated from its absorbance at 340 nm, using a molar extinction coefficient of 6200 M^{-1} cm^{-1} (*21*). Two values for the extinction coefficient of NADP at 260 nm, i.e., 15,300 M^{-1} cm^{-1} (*26*) and 18,000 M^{-1} cm^{-1} (*27*), have been reported; we employed a glucose-6-phosphate dehydrogenase assay (*28*) to determine $\epsilon_{260,NADP}$ and obtained a value of 18,800 M^{-1} cm^{-1}, and this was used to quantify NADP. The concentrations of GSSG solutions were quantified from their absorbance at 248 nm using an extinction coefficient of 382 M^{-1} cm^{-1} (*29*).

Macroscopic Redox Potentials of DmTrxR. The redox potentials of DmTrxR were determined by redox titrations (*11*, *12*) and steady-state kinetics (*49*, *50*). For redox titrations, NADH instead of NADPH was used as the titrant to avoid binding effects of NADP(H) on the measurements of the redox potential. DmTrxR (12−22 μM) in 0.1 M potassium phosphate buffer, 0.3 mM EDTA, pH 7.0, was contained in a cuvette having a syringe port and a stopcock; the solution was made anaerobic using alternating cycles of vacuum and argon. A separate solution of NADH containing either 1 equiv/20 μL or 1 equiv/50 μL was also made anaerobic by flushing with high purity argon for 30 min. A gastight Hamilton syringe was used to dispense the anaerobic solution of NADH into the enzyme solution, and the mixture was allowed to equilibrate at 25 °C between additions. From spectra recorded between 300 and 800 nm, equilibration was ascertained by following the absorbance at 462 and 540 nm (ideal wavelengths respectively for observation of FAD reduction and formation of the thiolate-FAD charge-transfer complexes of EH_2 or EH_4) until no further changes could be detected. At equilibrium, E_{ox} was quantified by the absorbance at 462 nm (A_{462}); EH_2 and EH_4 were quantified by both ΔA_{462} and ΔA_{540} using the corresponding $\Delta\epsilon$ values at 462 and 540 nm (see Results and Discussion for the detailed quantification). The equilibrium constants of the reaction E_{ox} + NADH ⇔ EH_2 + NAD were obtained using eq 1, and those of the reaction EH_2 + NADH ⇔ EH_4 + NAD were obtained using eq 2.

$$K_{eq,E_{ox}/EH_2,NAD/NADH} = \frac{[NAD]_{eq}[EH_2]_{eq}}{[NADH]_{eq}[E_{ox}]_{eq}} \quad (1)$$

$$K_{eq,EH_2/EH_4,NAD/NADH} = \frac{[NAD]_{eq}[EH_4]_{eq}}{[NADH]_{eq}[EH_2]_{eq}} \quad (2)$$

According to the Nernst principle, when a redox reaction reaches equilibrium, all redox couples in the system will be poised at an identical potential, E_h. Equation 3 gives the Nernst relationship for the two-electron reduction of the enzyme (E_{ox}/EH_2) by NADH, and eq 4 restates the relationship in terms of the equilibrium constant, K_{eq}. A similar relationship is given for the reaction of the EH_2/EH_4 couple with the NAD/NADH couple in eq 5. In the calculation of the redox potentials of the E_{ox}/EH_2 and EH_2/EH_4 couples using eqs 4 and 5, the NAD/NADH redox couple (E_m = −315 mV, at pH 7.0, 25 °C) is from refs *11* and *12*. All redox potential determinations were carried out at pH 7, and the values reported are given as at pH 7.

$$E_h = E_{m,NAD/NADH} + \frac{RT}{nF}\ln\frac{[NAD]_{eq}}{[NADH]_{eq}} = E_{m,E_{ox}/EH_2} + \frac{RT}{nF}\ln\frac{[E_{ox}]_{eq}}{[EH_2]_{eq}} \quad (3)$$

$$E_{m,E_{ox}/EH_2} = E_{m,NAD/NADH} + \frac{RT}{nF}\ln\frac{[NAD]_{eq}[EH_2]_{eq}}{[NADH]_{eq}[E_{ox}]_{eq}} = E_{m,NAD/NADH} + \frac{RT}{nF}\ln K_{eq,\,E_{ox}/EH_2,NAD/NADH} \quad (4)$$

$$E_{m,EH_2/EH_4} = E_{m,NAD/NADH} + \frac{RT}{nF}\ln\frac{[NAD]_{eq}[EH_4]_{eq}}{[NADH]_{eq}[EH_2]_{eq}} = E_{m,NAD/NADH} + \frac{RT}{nF}\ln K_{eq,EH_2/EH_4,NAD/NADH} \quad (5)$$

Steady-state kinetics methods, as have been described previously (*49*, *50*), were also used to measure the $E_{m,EH_2/EH_4}$ of the DmTrxR-catalyzed reactions. All measurements were carried out in 0.1 M potassium phosphate buffer, 0.3 mM EDTA, pH 7.0, 25 °C. When DmTrx-2 (3.5−72 μM) was the electron acceptor, reaction rates were monitored by the decrease in A_{340} due to the oxidation of NADPH (1.5−100 μM); in the reverse direction, where NADP (5−150 μM) was the electron acceptor, the increase in A_{340} due to reduction of NADP in the presence of Trx-$(SH)_2$ (3.5−72 μM) was monitored. A constant level of Trx-$(SH)_2$ was maintained by including 8 mM DTT in the buffer (*49*). In the case of the NADH + Trx-$(S)_2$ ⇔ NAD + Trx-$(SH)_2$ reaction, the concentrations of DmTrx-2 ranged from 3.5 to 72 μM, and those of NADH and NAD were 50 to 600 μM and 0.2 mM to 6.0 mM, respectively. Direct reductions of NADP or NAD by TrxR in the presence of 8 mM DTT but without Trx-$(S)_2$ were recorded for background correction;

the contributions of DTT to the initial rates of NADP reduction were found to be no more than 12%, and those for NAD reduction were no more than 8% of those in the presence of Trx-2. The steady-state kinetic parameter k_{cat}/K_m represents the apparent second-order rate constant of the reaction of substrate with the free enzyme. Using the Haldane equation, the equilibrium constants can be calculated, and the redox potential of the enzyme is then calculated with the Nernst equation (*49*, *50*). The results obtained by this method are expected to reinforce the results obtained by redox titrations in which EH_2 and EH_4 share considerable spectral similarities, and are therefore difficult to quantitatively evaluate.

Improved Methodology for the Determination of K_{eq}(s) and Redox Potentials of Trx(s). DmTrxR catalyzes the reversible reaction between NADPH and DmTrx as described by eq 6.

$$\text{DmTrx-(S)}_2 + \text{NADPH} + \text{H}^+ \overset{\text{DmTrxR}}{\rightleftharpoons} \text{NADP}^+ + \text{DmTrx-(SH)}_2 \quad (6)$$

Starting with solutions containing various initial ratios of the reactants, [NADP][Trx-$(SH)_2$]/[NADPH][Trx-$(S)_2$], a small volume of TrxR was added to permit the approach to equilibrium, and this reaction was followed by the absorbance changes at 340 nm that were due to the consumption or generation of NADPH. Concentrations of each of the reactants at equilibrium could be calculated using the stoichiometry of eq 6 to yield K_{eq}. Details of the method are described more fully in Results and Discussion. The redox potentials were calculated from the K_{eq} values using the Nernst equation. The redox potential of the NADP/NADPH couple was taken as −327 mV for the experiments reported here at ionic strength 0.282 and pH 7.0 (*30*). Although the measurements were carried out under aerobic conditions, control experiments under an argon atmosphere gave results that were identical, within experimental error. All the E_m values reported represent the average of at least two independent experiments. The working buffer was 0.1 M potassium phosphate, 0.3 mM EDTA, pH 7.0; NADPH solutions were made in 10 mM unneutralized Tris (*11*).

Reactivity of the DmTrx System with Glutathione. To develop a comprehensive picture of the reactivity of GSSG with the DmTrx system, we compared three different assays (*2*, *13*, *31*). (i) Anaerobic titration to study the direct reaction between GSSG and reduced DmTrxR (EH_4): EH_4 (22 μM) was prepared with $NaBH_4$ (*6*), and the titration by GSSG was carried out in the same way as described above for the titration of E_{ox} with NADPH. The titration was also performed with a catalytic amount of DmTrx-2 (0.2 μM) included to test if it was required for the coupling of GSSG to EH_4. (ii) The kinetics of GSSG reduction by NADPH catalyzed by DmTrxR to study the function of DmTrx-2 to shuttle electrons: The reaction between GSSG (168 μM) and NADPH (108 μM) was observed at 340 nm in the presence of 1.1 or 22 μM DmTrx-2 and 0.1 M potassium phosphate (pH 7.0, 25 °C); DmTrxR was added to a final concentration of 8.0 nM to start the reaction. (iii) This assay was carried out exactly as was assay (ii) except that the GSSG was not added until the reaction between NADPH and DmTrx-2 had come to equilibrium. In assays (ii) and (iii), the second addition of reagents caused less than 0.5% changes to the total volume of the reaction mixture.

RESULTS AND DISCUSSION

Redox Potentials of DmTrxR. The function of DmTrxR is to transfer electrons from NADPH to Trx-$(S)_2$. To understand how DmTrxR catalyzes the reduction of thioredoxin and participates in the GSSG-cycling process, it is essential to resolve the relationships between the catalytic properties and the redox properties. The macroscopic redox potentials of the E_{ox}/EH_2 and EH_2/EH_4 couples are particularly relevant because they are the major functional intermediates of DmTrxR in catalysis. As described above and shown in Scheme 1, the reducing equivalents in the EH_2 and EH_4 forms of the enzyme can reside on the flavin, or either of the two cysteine pairs, depending on their relative redox potentials. This leads to several forms of EH_2, namely, EH_2^A, EH_2^B, EH_2^C, and EH_2^D, and to two forms of EH_4, namely, EH_4^A and EH_4^B, which are elaborated in Scheme 1. Thus, the macroscopic redox potentials involve several species.

Rapid-reaction data from a previous study demonstrated that the reactions of 1 equiv of NADPH with wild-type DmTrxR or with the C-terminal mutants, C489S, C490S, or C489S/C490S, gave very similar kinetic profiles consisting of two phases (90−120 s^{-1} for flavin reduction by NADPH to form EH_2^A, and 49 s^{-1} as the nascent $FADH^-$ reduced the N-terminal disulfide to form EH_2^B) (*6*). The reactions with 2, 3, and 5 equiv of NADPH clearly led to a third phase (21 s^{-1}) for wild-type DmTrxR, but not for the mutants. This third phase corresponded to the reaction of a second equivalent of NADPH with EH_2, driving the system through EH_2^D as dithiol−disulfide exchange from the N-terminal dithiol to the C-terminal disulfide (on the other subunit) occurs, and forming EH_4, primarily in the form of EH_4^B (Scheme 1). Therefore, less than 1 equiv of NADPH will mainly convert E_{ox} to EH_2, and additional NADPH converts EH_2 to EH_4 (*6*). As shown in Figure 1, titration of DmTrxR with NADH (a nonphysiological substrate with little tendency to bind) caused a decrease in the absorbance at 462 nm (A_{462}) and an increase at 540 nm (A_{540}). The ΔA_{462} corresponds to the reduction of FAD in DmTrxR, while the ΔA_{540} indicates the formation of a thiolate−FAD charge-transfer complex (CTC) (*6*, *11*, *12*). Correlating these spectral changes to the model of the catalytic mechanism of DmTrxR in Scheme 1 (*6*), EH_2^B, the charge-transfer complex, appears to be the predominant species among the four EH_2 isoforms, and EH_4^B is the major species of the two EH_4 isoforms. The ΔA_{462} and ΔA_{540} observed during reduction reactions were used for quantifying E_{ox}, EH_2, and EH_4, from which K_{eq} and E_m can be calculated. The titration of DmTrxR with NADH shown in Figure 1A demonstrates four isosbestic points (360, 398, 440, and 505 nm) as the enzyme converts from the oxidized to its EH_2 forms; the A_{360} of spectrum 5 reflects the accumulation of unreacted NADH. During the titration of DmTrxR with 0−10 eq NADH, we observed three distinct phases. In the plot of A_{340} vs NADH, the slope is 0.004 from 0 to 1 equiv, and 0.022 between 1 and 2 equiv (Figure 1B). From 2 to 10 equiv, the slope is 0.0497, essentially the same as when NADH was added to phosphate buffer in the same way (slope = 0.0501). Therefore, in the titration the conversion of EH_2 to EH_4 by NADH is still considerable up to 2 equiv of NADH after the breakpoint at 1 equiv.

For the 2-electron reduction reaction (eq 7), eqs 8−11 were applied to approximate the concentration of each species at equilibrium.

$$E_{ox} + NADH \Leftrightarrow EH_2 + NAD \quad (7)$$

$$[NADH]_{eq} = \frac{A_{360obs} - A_{360,E_{ox}}}{\epsilon_{360,NADH}} \quad (8)$$

$$[EH_2]_{eq} = \frac{A_{540obs} - A_{540,E_{ox}}}{\Delta\epsilon_{540,EH_2/E_{ox}}} \text{ or } \frac{A_{462,E_{ox}} - A_{462obs}}{\Delta\epsilon_{462,EH_2/E_{ox}}} \quad (9)$$

$$[NAD]_{eq} = [EH_2]_{eq} \quad (10)$$

$$[E_{ox}]_{eq} = [E]_{total} - [EH_2]_{eq} \quad (11)$$

For the reduction to the 4-electron state (eq 12), eqs 13−16 were applied to approximate the concentration of each species at the equilibrium.

$$EH_2 + NADH \Leftrightarrow EH_4 + NAD \quad (12)$$

$$[NADH]_{eq} = \frac{A_{360obs} - A_{360,EH_2}}{\epsilon_{360,NADH}} \quad (13)$$

$$[EH_4]_{eq} = \frac{A_{540obs} - A_{540,EH_2}}{\Delta\epsilon_{540,EH_4/EH_2}} \text{ or } \frac{A_{462,EH_2} - A_{462obs}}{\Delta\epsilon_{462,EH_4/EH_2}} \quad (14)$$

$$[NAD]_{eq} = [E]_{total} + [EH_4]_{eq} \quad (15)$$

$$[EH_2]_{eq} = [E]_{total} - [EH_4]_{eq} \quad (16)$$

Throughout the above equations, $\epsilon_{360,NADH} = 4.1 \times 10^3$ M^{-1} cm^{-1}; $\Delta\epsilon_{540,EH_2/E_{ox}}$ is the extinction change at 540 nm from E_{ox} to EH_2 (2.7×10^3 M^{-1} cm^{-1}), and $\Delta\epsilon_{462,EH_2/E_{ox}}$ is the extinction change at 462 nm from E_{ox} to EH_2 (2.4×10^3 M^{-1} cm^{-1}); $\Delta\epsilon_{540,EH_4/EH_2}$ is the extinction change at 540 nm from EH_2 to EH_4 (4.0×10^2 M^{-1} cm^{-1}), and $\Delta\epsilon_{462,EH_2/EH_4}$ is the extinction change at 462 nm from EH_2 to EH_4 (4.2×10^2 M^{-1} cm^{-1}) (see Figure 1B and Materials and Methods). A_{360,EH_2}, A_{540,EH_2}, and A_{462,EH_2} represent the absorbance of the titration mixture at 360, 540, and 462 nm, respectively, when 1.0 equiv of NADH had reacted (quantitatively). Table 1 gives the redox potentials of the E_{ox}/EH_2 and EH_4/EH_2 couples calculated from data obtained at different wavelengths using eqs 1 and 2 to calculate K_{eq}, and the Nernst eq 3 to calculate E_m. There is no significant statistical difference between the two group values ($p > 0.01$ by t test). These two parallel assays gave an average value of −272 mV for $E_{m,E_{ox}/EH_2}$ and −298 mV for $E_{m,EH_2/EH_4}$, with standard deviations of 5 and 11 mV, respectively.

Because EH_2 and EH_4 have very similar spectra (Figure 1A), the measurement of $E_{m,EH_2/EH_4}$ did not have the accuracy achieved in the determination of $E_{m,E_{ox}/EH_2}$; therefore, we used a nonspectroscopic method to confirm this value. According to the Haldane relationship, the ratio of bimolecular rate constants of the forward direction to those of the back direction will give the equilibrium constant (K_{eq}^{app}) of a reaction. For the reductive half-reaction, NADPH + $DmTrxR_{ox}$ ⇔ NADP + $DmTrxR_{red}$, the K_{eq}^{app} can be calculated as the ratio of the k_{cat}/K_m for the forward reaction to that for reverse reaction; for the oxidative half-reaction DmTrx-$(S)_2$ + $DmTrxR_{red}$ ⇔ DmTrx-$(SH)_2$ + $DmTrxR_{ox}$, the K_{eq}^{app} can be calculated similarly as the ratio of the k_{cat}/K_m value for the reaction in one direction to that for the reaction in the other direction (*49*, *50*). It is essential to note that these relationships hold only when $[S] \ll K_m$, and therefore $[E]_{free} \sim [E]_{total}$ (*51*). It has been shown that the enzyme cycles in catalysis between EH_2 and EH_4 (*6*, *49*, *50*); it is reasonable to approximate k_{cat}, K_m, and k_{cat}/K_m from the enzyme-catalyzed steady-state reaction between NADPH and DmTrx-$(S)_2$ or from that between DmTrx-$(SH)_2$ and NADP. The K_{eq}^{app} values obtained in this way are thus the equilibrium constant of the reaction of NADPH with EH_2 (NADPH + EH_2 ⇔

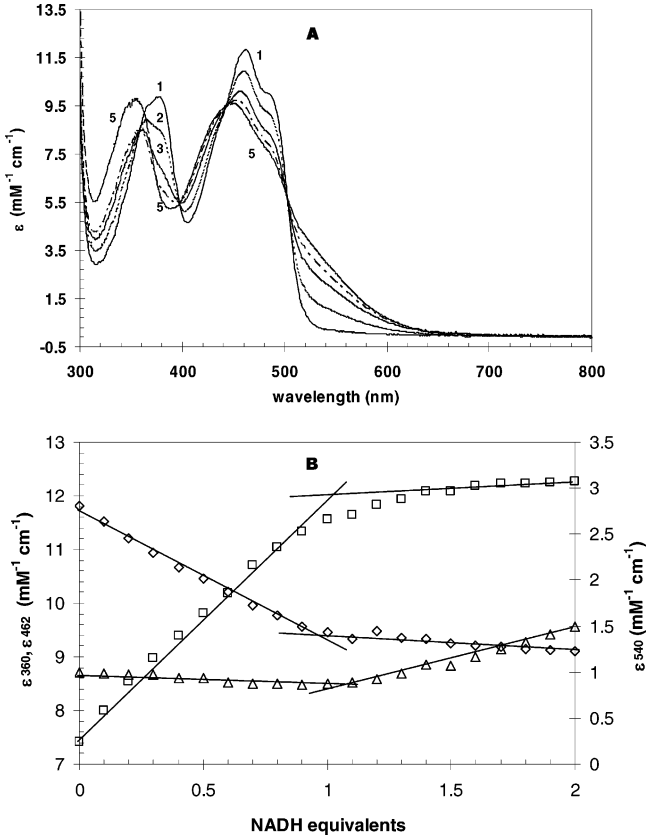

FIGURE 1: The titration of DmTrxR with NADH. The titration was conducted anaerobically at 25 °C, in 0.1 M phosphate buffer, pH 7.0. DmTrxR was at a final concentration of 22 μM. (A) Spectra 1−5 were taken for the enzyme when 0, 0.3, 0.7, 1.0, and 2.0 equiv of NADH were used for titration. Spectral changes were complete in less 10 min, and no further change in the spectrum was observed in 2 h. (B) The typical changes in absorbance at 462 nm (◇), 360 nm (△), and 540 nm (□) during the titration with NADH.

Table 1: The Macroscopic Redox Potentials (mV) of DmTrxR Measured by Redox Titration with NADH at pH 7.0, 25 °C ($n = 4$)

measurement	$E_{m,E_{ox}/EH_2}$	$E_{m,EH_2/EH_4}$
based on A_{360} and A_{540}	−273 ± 2	−296 ± 8
based on A_{360} and A_{462}	−271 ± 7	−299 ± 17
average	−272 ± 5	−298 ± 11
		−293 ± 15,[a] −290 ± 8[b]

[a] The redox potential determined in this work by steady-state kinetics of DmTrxR-catalyzed reaction, NADPH + Trx-$(S)_2$ ⇔ NADP + Trx-$(SH)_2$. The average was taken of −303 mV and −282 mV as shown in Table 2. [b] The redox potential determined in this work by steady-state kinetics of DmTrxR-catalyzed reaction, NADH + Trx-$(S)_2$ ⇔ NAD + Trx-$(SH)_2$. The average was taken of −284 mV and −295 mV as shown in Table 2.

Table 2: The Determination of $E_{m,EH_2/EH_4}$ by Steady-State Kinetics[a]

NADPH + Trx-$(S)_2$ ⇔ NADP + Trx-$(SH)_2$				
	NADPH	NADP	Trx-$(S)_2$	Trx-$(SH)_2$
K_m (μM)	3.7 ± 0.3	9.4 ± 0.2	5.7 ± 0.6	3.6 ± 0.5
k_{cat} (min^{-1})	1243 ± 21	481 ± 24	1243 ± 21	481 ± 24
k_{cat}/K_m (min^{-1} μM^{-1})	341 ± 28	51 ± 1	219 ± 24	137 ± 18
K_{eq}^{app}	6.7 ± 0.7		0.63 ± 0.04	
$E_{m,EH_2/EH_4}$ (mV)	−303 ± 1 −301 ± 3[b]		−282 ± 1 −281 ± 10[b]	

NADH + Trx-$(S)_2$ ⇔ NAD + Trx-$(SH)_2$				
	NADH	NAD	Trx-$(S)_2$	Trx-$(SH)_2$
K_m (mM)	0.22 ± 0.04	11.7 ± 0.04	8.0 ± 1.3[c]	8.6 ± 1.5[c]
k_{cat} (min^{-1})	17.1 ± 0.3	86.2 ± 0.8	17.1 ± 0.3	86.2 ± 0.8
k_{cat}/K_m (min^{-1} mM^{-1})	81 ± 13	7.4 ± 0.7	2.2 ± 0.4[d]	10.3 ± 1.8[d]
K_{eq}^{app}	11 ± 2		4.7 ± 0.3	
$E_{m,EH_2/EH_4}$ (mV)	−284 ± 2		−295 ± 3	

[a] Experimental conditions are described in Materials and Methods. [b] The redox potentials of EH_2/EH_4 for rat TrxR determined by steady-state kinetics with NADPH and *C. reinhardtii* Trx as the substrates at pH 7.0, 25 °C (*49*). The authors of ref 49 obtained a redox potential of −294 mV with a reference potential for NADPH of −320 mV rather than −327 mV (*30*). The value here is recalculated using −327 mV as the reference potential for NADPH. [c] The unit of K_m is μM for Trx-$(S)_2$ and Trx-$(SH)_2$. [d] The unit of k_{cat}/K_m is min^{-1} μM^{-1} for Trx-$(S)_2$ and Trx-$(SH)_2$.

NADP + EH_4), or of the reaction of DmTrx-$(S)_2$ with EH_4 (DmTrx-$(S)_2$ + EH_4 ⇔ DmTrx-$(SH)_2$ + EH_2), respectively. The value of K_{eq}^{app} will then yield the redox potential of the EH_2/EH_4 couple because it is directly related to the difference (ΔE_m) between $E_{m,substrate}$ and the $E_{m,EH_2/EH_4}$. This relationship is shown in eq 17, which was derived from eq 5 for the reaction between EH_2/EH_4 and NADP/NADPH; the relationship also holds for the reaction between EH_2/EH_4 and DmTrx-$(S)_2$/DmTrx-$(SH)_2$.

$$\Delta E_m = E_{m,EH_2/EH_4} - E_{m,NADPH/NADP} = \frac{RT}{nF} \ln \frac{[NADP]_{eq}[EH_4]_{eq}}{[NADPH]_{eq}[EH_2]_{eq}} = \frac{RT}{nF} \ln K_{eq,EH_2/EH_4,NADP/NADPH} \quad (17)$$

Both NADPH and NADH were used as reducing substrates, and DmTrx2 was used as the oxidizing substrate (E_m = −275.4 mV as determined in the following section). The parameters obtained from the steady-state kinetics of the DmTxrR-catalyzed reactions between DmTrx2 and NAD(P)H are listed in Table 2, and the redox potential of EH_2/EH_4 was calculated accordingly. The average values of the redox potentials in both cases (−293 ± 15 mV and −290 ± 8 mV when NADPH and NADH act as the reducing substrate, respectively) agree fairly well with the redox potential obtained using spectral titration data (−298 ± 11 mV), (Table 1). Therefore, we believe the results from both methods are reliable; $E_{m,E_{ox}/EH_2}$ and $E_{m,EH_2/EH_4}$ from the same method (redox titration) will be used in the following discussion. It should be noted that the $E_{m,EH_2/EH_4}$ values calculated with different redox references give some variation (Table 2); e.g., the steady-state kinetics of the DmTrxR catalyzed reaction, NADPH + Trx-$(S)_2$ ⇔ NADP + Trx-$(SH)_2$, gave an $E_m(EH_2/EH_4)$ of −303 mV with NADP/NADPH as the redox reference, and −282 mV with Trx-$(S)_2$/Trx-$(SH)_2$. A similar phenomenon was observed in the case of rat TrxR (*49*), where NADPH and *Chlamydomonas reinhardtii* Trx were used as the substrates and redox references. Substrate/product inhibition is very likely one cause of this phenomenon (*49*, *52*). Mixed inhibition by NADP has been reported for rat TrxR and indeed is a characteristic of ping-pong reactions; the competitive binding of NADP (vs NADPH) to TrxR (*49*) and the resultant reoxidation of EH_4 to EH_2 by NADP after its binding may account for the mixed inhibition (N. Cenas personal communication). In addition, the binding of NADP to the several isoforms of reduced enzyme (EH_2^A, EH_2^B, EH_2^C, EH_2^D, EH_4^A, and EH_4^B) may not be identical; thus, the differential binding properties of NADP could also lead to a shift in the equilibrium between EH_2 and EH_4. This kind of inhibition will affect the initial rate of the TrxR-catalyzed reactions between Trx and NAD(P)H, from which the ratio of k_{cat}/K_m and $E_{m,EH_2/EH_4}$ were obtained. Furthermore, E_{ox} must be reduced to EH_2 prior to catalysis; the velocities of this reaction will be different depending on the reductant (Trx-$(SH)_2$, NADH, or NADPH). These differences could influence the observed initial rates of the DmTrxR catalyzed reactions between NAD(P)H and Trx-$(S)_2$. Again, because both k_{cat} and K_m were obtained from the initial phases of the TrxR-catalyzed reactions, any deviation in the initial step of $E_{ox} \rightarrow EH_2$ would cause the deviation in K_{eq}^{app} measurements and $E_{m,EH_2/EH_4}$ calculations.

The redox potential of the NADP/NADPH couple was reported as −327 mV (*30*), considerably more negative than that of E_{ox}/EH_2 (−272 mV), so that the formation of EH_2 is greatly favored. On the other hand, the redox potential of EH_2/EH_4 (∼−298 mV) is closer to that of NADP/NADPH, indicating a $K_{eq,EH_2/EH_4,NADP/NADPH}$ of 9.5 (according to eq 2), a value reasonably near that determined, 6.7 (Table 2). The differences in potentials of these redox couples appear to be correlated with their reactivities. The ΔE_m for E_{ox}/EH_2 vs NADP/NADPH is 55 mV, whereas the ΔE_m for EH_2/EH_4 vs NADP/NADPH is 29 mV. Consistent with this, the reaction of NADPH with E_{ox} (95−120 s^{-1}) is considerably faster than the reaction of NADPH with EH_2 (21 s^{-1}) (*6*). The redox potential for the EH_4/EH_6 couple was assumed to be as low as −400 mV (*6*), implying an equilibrium constant of 3.4 × 10^{-3} (ΔE_m = −73 mV relative to the NADPH/NADP couple). Thus, the reduction of EH_4 by NADPH is not favored either thermodynamically or by extension, kinetically. When NADH was used as a reductant, where no binding effects should be present, even 10 equiv of titrant did not induce significant reduction of EH_4 (data not shown), which is consistent with the proposal that EH_6 is not involved in the catalysis cycle.

Determination of E_m (Trx). The reaction between oxidized thioredoxin and NADPH is reversible in the presence of TrxR (Figure 2). When mixtures containing Trx-$(S)_2$, Trx-$(SH)_2$, NADPH, and NADP are allowed to come to equilibrium in the presence of DmTrxR, changes observed in the NADPH concentration permit final concentrations of each reactant to be determined. The equilibrium constant (K_{eq}) can be calculated according to the stoichiometry shown in eq 6; the proton concentration was omitted in calculations of K_{eq} at

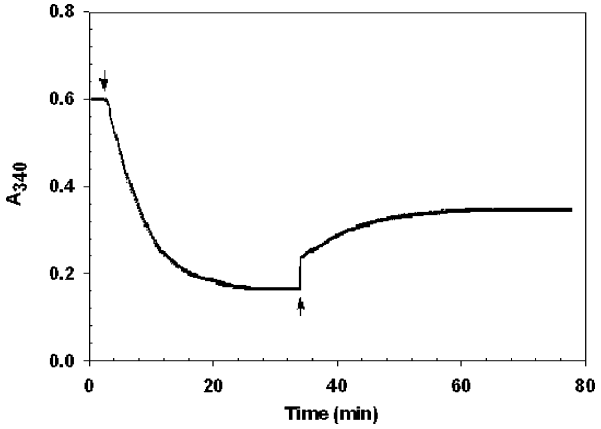

FIGURE 2: The reversible TrxR-catalyzed reaction between DmTrx-2 and NADPH. Starting with DmTrx-2 (100 μM) and NADPH (100 μM) in 1 mL of 0.1 M phosphate buffer, 0.3 mM EDTA, pH 7.0, 25 °C, the reaction was initiated by adding 5 μL of 8.4 μM DmTrxR, (shown at the first arrow). When the first equilibrium was established, 10 μL of $NADP^+$ (100 mM) was added (shown at the second arrow) and a second equilibrium was established.

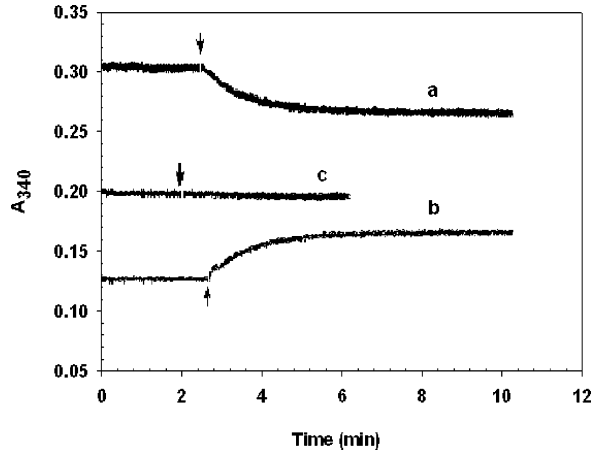

FIGURE 3: Examples of the improved method to determine K_{eq}. Starting with different initial ratios, [NADP][Trx-$(SH)_2$]/[NADPH][Trx-$(S)_2$], the reaction was triggered by adding 2 μL of TrxR (final concentration = 40 nM). (a) When the initial ratio is $>K_{eq}$, reaction 6 proceeds in the forward direction and consumption of NADPH is observed as a decrease in A_{340}. (b) When the initial ratio is $<K_{eq}$, the reaction proceeds in the reverse direction, and NADPH is produced as indicated by an increase in A_{340}. (c) When the initial ratio equals K_{eq}, the absorbance at 340 nm does not change, showing that no net reaction occurs. The arrows indicate where DmTrxR was added to initiate the reactions.

pH 7.0, the value used in these assays. In principle, measured K_{eq} values should be identical for a given system regardless of what starting concentrations are used, or from which directions the reaction approaches equilibrium. However, K_{eq} determined from the first equilibrium in Figure 2 is much lower (3.5 $\pm$ 0.2) than K_{eq} from the second equilibrium (21.8 $\pm$ 3.5). The large difference in these values most likely derives from the initial concentrations in the first case being far from equilibrium, making the data less reliable. Moreover, inhibition of TrxR by NADPH (*52*) and by NADP (*49*) may lead to an inaccurate value for K_{eq}.

We avoided these potential pitfalls of using initial ratios that are far from equilibrium by applying an approach analogous to that described previously (*33, 34*) and illustrated in Figure 3. An estimate of K_{eq} is first obtained by carrying out a series of experiments as shown in Figure 3, systematically varying initial concentrations of the reactants to achieve a series of ratios that bracket the true K_{eq}. Thus, absorbance changes in both directions are observed. The change in absorbance at 340 nm observed as the reaction comes to equilibrium is plotted vs the initial ratio of reactants before adding TrxR, as shown in Figure 4. The data are extrapolated to provide an estimate of what ratio gives no net change in absorbance, and this is assumed to be the equilibrium ratio. To improve the accuracy of this determination, this procedure can be repeated using a series of ratios that are closer to the K_{eq} estimated from the first survey. The concentrations of reactants are chosen to provide limited, but readily observable, net reactions, with ratios of reactants that result in the reaction approaching equilibrium from each direction (Figure 3). Thus, the final determination avoids using ratios far from equilibrium.

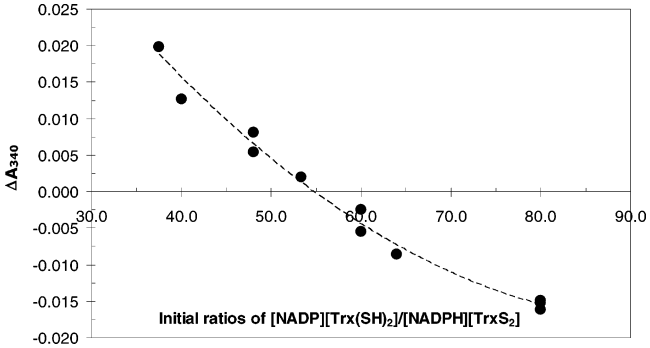

FIGURE 4: Plot of the change in A_{340} for the reaction to come to equilibrium vs the initial ratios of reactants. The crossover point where the change in A_{340} is zero gives the K_{eq} value. Shown herein is the data for determining K_{eq} for DmTrx-2 in 0.1 M potassium phosphate buffer containing 0.3 mM EDTA at pH 7.0, 25 °C . The initial ratio of [DmTrx-$(SH)_2$]/[DmTrx-$(S)_2$] was kept constant at 5. The initial concentrations of NADPH and NADP were varied systematically to give the ratios of [NADP]/[NADPH] from 7.5 to 16, but the sum of the concentrations of NADP + NADPH was maintained at 220 μM. The initial ratios of [NADP][DmTrx-$(SH)_2$]/[NADPH][DmTrx-$(S)_2$] ranged from 37.5 to 80 accordingly.

The initial reactant concentrations have been varied systematically in two ways. First as shown in Figure 4, the initial ratio of [DmTrx-$(SH)_2$]/[DmTrx-$(S)_2$] was kept constant at 5, and the initial concentrations of NADPH and NADP were changed systematically, but with the initial total concentration of NADPH + NADP maintained at 220 μM. Alternatively, the initial ratio [NADP]/[NADPH] was kept constant at 8 and the initial concentrations of DmTrx-$(SH)_2$ and DmTrx-$(S)_2$ were varied systematically to yield ratios of [DmTrx-$(SH)_2$]/[DmTrx-$(S)_2$] from 5.5 to 8.8 while keeping their total concentration constant at 70 μM. To obtain a smooth line such as that shown in Figure 4, the ratio of one of the reagent pairs should be maintained constant, while the other is varied, but the sum of their concentrations is held constant. Otherwise a smooth simple trend is unlikely to be obtained, and the crossover point will be more difficult to discern. The K_{eq} values were also calculated from each of the [NADP][Trx-$(SH)_2$]/[NADPH][Trx-$(S)_2$] ratios measured at equilibrium from the data in Figure 4. As expected, because all of the initial conditions used in this plot were close to the K_{eq}, the average K_{eq} value from this set agreed closely with that obtained from the crossover point. The results in Table 3 demonstrate that the redox potentials determined here agree well with those reported previously.

Table 3: Determination of the K_{eq} and E_m of Thioredoxins Using the Improved Approach (at pH 7.0, 25 ± 0.4 °C)

	K_{eq}[a]		E_m (mV)[b]	
	in this work	reported	in this work	reported
DmTrx-2	56 ± 1.0		−275.4 ± 0.3	
EcTrx	28.2 ± 2.1	48 (*35*)	−284.2 ± 1.0	−285 (*30*, *35*)
				−283 (*30*, *36*)
PfTrx	74 ± 2.4	110 ± 10 (*13*)	−271.9 ± 0.4	−270 (*13*)

[a] The K_{eq} was calculated as the ratio of [NADP][Trx-$(SH)_2$]/[NADPH][Trx-$(S)_2$] when the equilibrium had been established for the reaction NADPH + Trx-$(S)_2$ ⇔ NADP + Trx-$(SH)_2$ catalyzed by TrxR. [b] E_m was calculated using the following equation: $E_{m,Trx} = E_{m,NADP} + [(RT)/(nF)](\ln K_{eq})$. The results confirm values reported in the literature for the redox potentials of thioredoxins from *E. coli* and from *P. falciparum*. The value of E_m calculated from the K_{eq} in ref 35 has been corrected for temperature from "room temperature," assumed to be 20 °C, to 25 °C (+7 mV). Corrections for the values taken from Moore et al. (*35*) and from Krause et al. (*36*) were applied as described by Lennon and Williams (*30*), resulting in a redox potential for $NADP^+$/NADPH of −327 mV at ionic strength of 0.28.

The reason for the big difference between the K_{eq} measured in this work and those reported previously is that the improved methodology overcomes many of the aforementioned pitfalls, and thus gives more precise results. The difference between the values of K_{eq} reported in this study and those reported earlier appears large compared to the difference in E_m values, because the logarithm of K_{eq} is used to calculate E_m.

A previous study from this lab indicated that DmTrx-$(S)_2$, when mixed with $NaBH_4$-reduced DmTrxR (EH_4), led to an increase in A_{462} (flavin reoxidation) and a concomitant decrease in A_{540} (CTC), but never restored the spectrum of fully oxidized DmTrxR, even after the addition of 4 equiv of DmTrx-$(S)_2$ (*6*). The failure to observe a spectrum of the fully oxidized DmTrxR is not surprising if the redox potentials of these species (as determined here) are taken into consideration. DmTrx-$(S)_2$/DmTrx-$(SH)_2$ shows a redox potential of −275.4 mV, very close to that of E_{ox}/EH_2 (−272 mV). The lack of driving force makes the electron transfer very slow between these two redox couples ($\Delta E_m = -3.4$ mV) (*37*), and is likely the main cause of the very slow kinetics (the second phase, 0.5 s^{-1}) shown in the oxidative half-reaction of DmTrxR (*6*). In contrast, a very fast phase was observed at the beginning of the oxidative half-reaction (140 s^{-1}), which corresponds to the reoxidation of EH_4 by DmTrx-$(S)_2$ ($\Delta E_m = 23$ mV). Therefore, the redox potentials determined here clearly give evidence that EH_2 and EH_4 are the catalytically active species. Although a tiny amount of E_{ox} and EH_6 might be formed during the reactions of DmTrxR with DmTrx2-$(S)_2$ or with NADPH, they are not likely to be major participants in the catalytic cycle.

Reactivity of the DmTrx System with Glutathione. *D. melanogaster* is deficient in glutathione reductase, and it has been proposed that the Trx system maintains a large value for the $(GSH)^2$/GSSG ratio via a nonenzymatic dithiol−disulfide interchange between Trx-$(SH)_2$ and GSSG (Scheme 1) (*2, 13*). To test this proposal, we have used three assays to determine how each component of the Trx system interacts with GSSG. Anaerobic titration of EH_4 by GSSG (assay i) can provide direct information about the electron transfer between the reduced DmTrxR and GSSG. Figure 5A shows that GSSG could not induce significant oxidization of EH_4

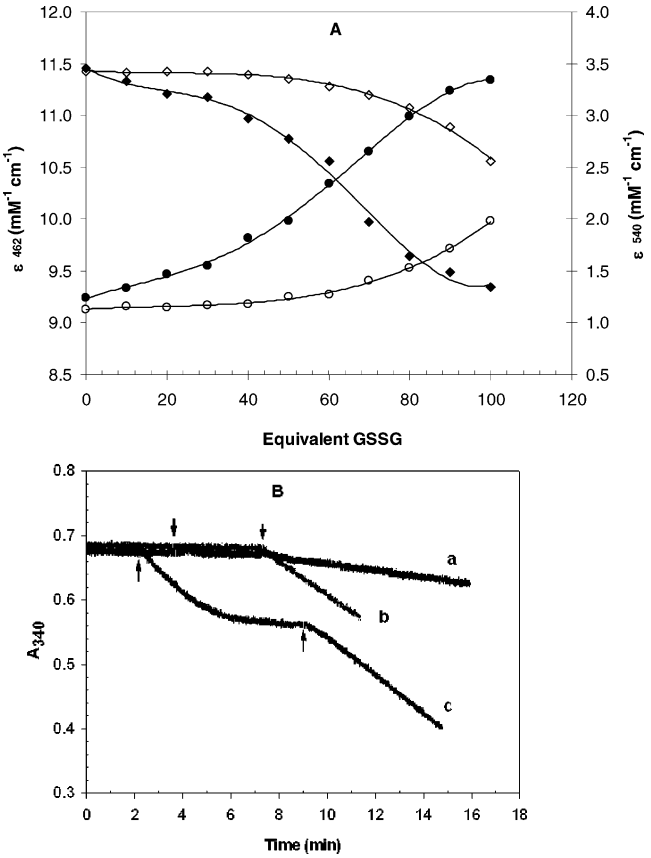

FIGURE 5: The reaction of GSSG with the DmTrx system. (A) The dependence of the oxidation of DmTrxR (EH_4) (22 μM) on the concentration of GSSG. The reactions were detected by the changes in absorbance at 462 nm (●, ○) and 540 nm (◆, ◇), in the presence (solid symbols) and absence (open symbols) of a catalytic amount of DmTrx-2 (0.2 μM). Each data point represents the extent of the reaction 30 min after GSSG addition. (B) The reaction of GSSG (168 μM) with NADPH (108 μM) catalyzed by DmTrxR (8 nM), in the presence of DmTrx-2 (a, 1.1 μM; b, 22 μM). The reaction was initiated by the addition of DmTrxR (8 nM at the first arrow); subsequent addition of DmTrx-2 (1.1 or 22 μM) is indicated by the second arrow. NADPH oxidation by GSSG was detected by the decrease in the absorbance at 340 nm. (c) This assay was carried out exactly as was assay b except that the GSSG was not added until the reaction between NADPH and DmTrx-2 had come to equilibrium (second arrow).

even when a 60-fold excess was used; however, in the presence of a catalytic amount of DmTrx-2 (0.2 μM), only 10 equiv of GSSG caused a discernible increase in ϵ_{462} (flavin oxidation) with a concomitant decrease in ϵ_{540} (disappearance of CTC). This indicates that DmTrxR cannot effectively utilize GSSG as its direct electron acceptor, but that the added DmTrx-2 (0.2 μM) mediates the electron transfer between EH_4 and GSSG.

The rate of NADPH oxidation by GSSG was observed in the second and third assays. The rate was dependent on the concentration of DmTrx-2 (Figure 5B); with DmTrx-2 at 1.1 μM the rate was 0.78 μM/min and at 22 μM the rate was 4.37 μM/min (traces a and b, respectively). This confirms the finding that GSSG cannot react directly with DmTrxR (Figure 5A); the reaction must be mediated by DmTrx-2. In the third assay, GSSG was not added until the reaction between NADPH and DmTrx-2 had come to equilibrium. As expected, when the DmTrxR-catalyzed reaction between NADPH and DmTrx-2 reached equilibrium, addition of GSSG led to further NADPH consumption at an

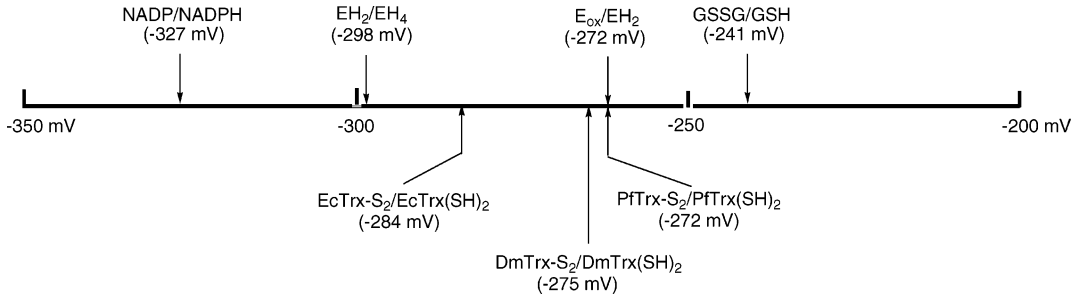

FIGURE 6: A scale showing the relative redox potentials of DmTrxR, DmTrx-2, PfTrx, EcTrx, GSSG, and NADPH at pH 7.0, 25 °C.

initial rate (6.08 μM/min) comparable to that induced by DmTrx-2 (5.13 μM/min) as shown in Figure 5B, trace c). From the results shown in Figure 5, it can be concluded that GSSG does not interact directly with DmTrxR; DmTrx-2 serves as an electron shuttle between EH_4 and GSSG (Scheme 1), thus permitting the reduction of GSSG by NADPH in this glutathione reductase-deficient insect.

The various redox systems under study here are compared on a redox scale in Figure 6. It can be seen that in a thermodynamic sense GSSG should be able to oxidize EH_4 to EH_2. However, a physical barrier must prevent GSSG from reacting with the C-terminal thiols of DmTrxR. The C-terminal 16-residue extension found in most high-M_r TrxRs (*8, 39*) is likely to block GSSG access in TrxR and prevent it from acting as a glutathione reductase (*8*). During catalysis, the flexible C-terminus approaches close enough to the N-terminal redox-active disulfide to promote electron transfer without steric clashes; after reduction, the C-terminal tail moves away from the catalytic site to a position at the surface of the enzyme where it can interact with the bound Trx-$(S)_2$. This C-terminal tail may prevent access of GSSG to the nascent N-terminal dithiol by occupying a possible glutathione-binding site (*2, 8, 13, 31*); however, the negative charges on GSSG may be the major deterrent to its binding.

Nature designates reduced DmTrx2 as the GSSG-cycling enzyme in *D. melanogaster* cells that lack GR so that redox homeostasis can be maintained. The fairly negative E_m values of EcTrx, DmTrx, and PfTrx compared to that of GSSG (Figure 6) support their biochemical functions very well. The rate constant for DmTrx-2 reducing GSSG is 170 M^{-1} s^{-1}, which allows high GSSG fluxes, on the order of 10 to 100 μM/min, and produces sufficiently high GSH concentrations in *D. melanogaster* cells to support homeostasis (*2*). Although PfTrx is slightly more oxidizing than DmTrx and EcTrx (Figure 6), PfTrx was better able to reduce GSSG than the other thioredoxins (*13*). This enhanced reactivity should arise at least in part from the favorable electrostatic interactions between GSSG and PfTrx, because the reaction rates also depend on electrostatic interactions (*13, 48*). The 3-dimensional structures of thioredoxins are known to be highly conserved (*40, 44, 45*, PDB ID code 1SYR for PfTrx structure); however, sequence alignment indicates a non-conserved amino acid close to the active site of PfTrx. A basic arginine is interposed between two highly conserved residues (Lys-36 and Ile-38) in PfTrx, whereas the particular residue in *E. coli* and in *D. drosophila* is the apolar methionine. Such a variation may strengthen the binding affinity of PfTrx with the negatively charged GSSG and enhance the affinity between PfTrx and GSSG to facilitate the dithiol−disulfide reaction (*29, 41−45*).

CONCLUDING REMARKS

This work shows that DmTrxR catalyzes the reversible transfer of reducing equivalents from NADPH to DmTrx-2. This process is consistent with the corresponding redox potentials and is essential for GSSG/GSH cycling in *D. Melanogaster*, which is deficient in glutathione reductase. The results of this work are fully consistent with EH_2 and EH_4 being the primary enzyme species in catalysis, and lend strong support to the proposed catalytic mechanism of DmTrxR and to the essential role of the DmTrx system in GSSG cycling. The redox potentials determined here indicate that NADPH can readily reduce E_{ox} to EH_2 and to EH_4, but not to EH_6; on the other hand, DmTrx2-$(S)_2$ can reoxidize EH_4 to EH_2, but it cannot reoxidize EH_2 to E_{ox}. GSSG fails to be a substrate of DmTrxR despite its more positive redox potential, presumably because it cannot properly access the TrxR C-terminal thiols. DmTrx-2 is required for interaction with DmTrxR, and it acts as a good carrier of reducing equivalents between DmTrxR and GSSG. This accomplishes GSSG/GSH cycling in the absence of glutathione reductase.

In addition, this work reports an improved approach for the determination of the K_{eq} values of TrxR-catalyzed reactions between Trx and NADPH. This approach effectively avoids the pitfalls of traditional methods in which the initial conditions are often far from equilibrium and lead to greater experimental uncertainty. In addition, it demonstrates the advantages of varying reagents in a systematic manner. The improved method was used to determine the redox potentials of DmTrx, EcTrx, and PfTrx, and gave results very consistent with the reported values.

ACKNOWLEDGMENT

We thank Drs. Bruce Palfey (University of Michigan, Ann Arbor, MI), Stephen Mayhew, (University College, Dublin), and Narimantas Cenas (Institute of Biochemistry, Vilnius, Lithuania) for discussions and helpful comments on the manuscript.

REFERENCES

1. Williams, C. H., Arscott, L. D., Muller, S., Lennon, B. W., Ludwig, M. L., Wang, P. F., Veine, D. M., Becker, K., and Schirmer, R. H. (2000) Thioredoxin reductase two modes of catalysis have evolved, *Eur. J. Biochem. 267*, 6110−6117.
2. Kanzok, S. M., Fechner, A., Bauer, H., Ulschmid, J. K., Muller, H. M., Botella-Munoz, J., Schneuwly, S., Schirmer, R., and Becker, K. (2001) Substitution of the thioredoxin system for glutathione reductase in Drosophila melanogaster, *Science 291*, 643−646.
3. Missirlis, F., Ulschmid, J. K., Hirosawa-Takamori, M., Gronke, S., Schafer, U., Becker, K., Phillips, J. P., and Jackle, H. (2002) Mitochondrial and cytoplasmic thioredoxin reductase variants

encoded by a single Drosophila gene are both essential for viability, *J. Biol. Chem. 277*, 11521−11526.
4. Arner, E. S. J., and Holmgren, A. (2000) Physiological functions of thioredoxin and thioredoxin reductase, *Eur. J. Biochem. 267*, 6102−6109.
5. Watson, W. H, Yang, X., Choi, Y. E., Jones, D, P., and Kehrer, J. P. (2004) Thioredoxin and its role in toxicology, *Toxicol. Sci. 78*, 3−14.
6. Bauer, H., Massey, V., Arscott, L. D., Schirmer, R. H., Ballou, D. P., and Williams, C. H. (2003) The mechanism of high M-r thioredoxin reductase from *Drosophila melanogaster*, *J. Biol. Chem. 278*, 33020−33028.
7. Zhong, L., Arner, and E. S., Holmgren, A. (2000) Structure and mechanism of mammalian thioredoxin reductase: the active site is a redox-active selenolthiol/selenenylsulfide formed from the conserved cysteine-selenocysteine sequence, *Proc. Natl. Acad. Sci. U.S.A. 97*, 5854−5859.
8. Sandalova, T., Zhong, L., Lindqvist, Y., Holmgren, A., and Schneider, G. (2001) Three-dimensional structure of a mammalian thioredoxin reductase: implications for mechanism and evolution of a selenocysteine-dependent enzyme, *Proc. Natl. Acad. Sci. U.S.A. 98*, 9533−9538.
9. Bauer, H., Kanzok, S. M., and Schirmer, R. H. (2002) Thioredoxin-2 but not thioredoxin-1 is a substrate of thioredoxin peroxidase-1 from Drosophila melanogaster—Isolation and characterization of a second thioredoxin in D-melanogaster and evidence for distinct biological functions of Trx-1 and Trx-2, *J. Biol. Chem. 277*, 17457−17463.
10. Holmgren, A., and Bjornstedt, M. (1995) Thioredoxin and thioredoxin reductase, *Methods Enzymol. 252*, 199−208.
11. Veine, D., M., Arscott, L. D., and Williams, C. H. (1998) Redox Potentials for Yeast, *Escherichia coli* and Human Glutathione Reductase Relative to the NAD^+/NADH Redox Couple: Enzyme Forms Active in Catalysis, *Biochemistry 37*, 15575−15582.
12. Krauth-Siegel, R. L., Arscott, L. D., Schonleben-Janas, A., Schirmer, R. H., and Williams, C. H. (1998) Role of active site tyrosine residues in catalysis by human glutathione reductase, *Biochemistry 37*, 13968−13977.
13. Kanzok, S. M., Schirmer, R. H., Turbachova, I., Iozef, R., and Becker, K. (2000) The thioredoxin system of the malaria parasite Plasmodium falciparum—Glutathione reduction revisited, *J. Biol. Chem. 275*, 40180−40186.
14. Veine, D. M., Mulrooney, S. B., Wang, P. F., and Williams, C. H. (1998) Formation and properties of mixed disulfides between thioredoxin reductase from Escherichia coli and thioredoxin: Evidence that cysteine-138 functions to initiate dithiol-disulfide interchange and to accept the reducing equivalent from reduced flavin, *Protein Sci. 7*, 1441−1450.
15. Aslund, F., Berndt, K. D., and Holmgren, A. (1997) Redox Potentials of Glutaredoxins and Other Thiol-Disulfide Oxidoreductases of the Thioredoxin Superfamily Determined by Direct Protein-Protein Redox Equilibria, *J. Biol. Chem. 272*, 30780−30786.
16. Darby, N. J., and Creighton, T. E. (1995) Characterization of the active site cysteine residues of the thioredoxin-like domains of protein disulfide isomerase, *Biochemistry 34*, 16770−16780.
17. Cline, D. J., Redding, S. E., Brohawn, S. G., Psathas, J. N., Schneider, J. P., and Thorpe, C. (2004) New Water-Soluble Phosphines as Reductants of Peptide and Protein Disulfide Bonds: Reactivity and Membrane Permeability, *Biochemistry 43*, 15195−15203.
18. Creighton, T. E. (1997) *Protein Structure: A Practical Approach*, Oxford University Press, New York.
19. Misenheimer, T. M., Huwiler, K. G., Annis, D. S., and Mosher, D. F. (2000) Physical Characterization of the Procollagen Module of Human Thrombospondin 1 Expressed in Insect Cells, *J. Biol. Chem. 275*, 40938−40945.
20. Berglund, O., and Sjöberg, B.-M. (1970) A Thioredoxin Induced by Bacteriophage T4. II. Purification and characterization, *J. Biol. Chem. 245*, 6030−6035.
21. Slaby, I., Cerna, V., Jeng, M.-F., Dyson, H. J., and Holmgren, A. (1996) Replacement of Trp in *Escherichia coli* Thioredoxin by Site-directed Mutagenesis Affects Thermodynamic Stability but Not Function, *J. Biol. Chem. 271*, 3091−3096.
22. Mahler, H. R., and Cordes, E. H. (1966) *Biological Chemistry*, Harper & Row, New York.
23. Sober, H. A. (1970) *Handbook of Biochemistry*, The Chemical Rubber Co., Cleveland, Ohio.
24. Davioud-Charvet, E., McLeish, M. J., Veine, D. M., Giegel, D., Arscott, L. D., Andricopulo, A. D., Becker, K., Muller, S., Schirmer, R. H., Williams, C. H. Jr., and Kenyon, G. L. (2003) Mechanism-based inactivation of thioredoxin reductase from Plasmodium falciparum by Mannich bases. Implication for cytotoxicity, *Biochemistry 42*, 13319−13330.
25. O'Donnell, M. E., and Williams, C. H., Jr. (1983) Proton stoichiometry in the reduction of the FAD and disulfide of Escherichia coli thioredoxin reductase. Evidence for a base at the active site, *J. Biol. Chem. 258*, 13795−13805.
26. Lin, T.-Y. (1999) G33D Mutant Thioredoxin Primarily Affects the Kinetics of Reaction with Thioredoxin Reductase. Probing the Structure of the Mutant Protein, *Biochemistry 38*, 15508−15513.
27. Chivers, P. T., and Raines, R. T. (1997) General Acid/Base Catalysis in the Active Site of *Escherichia coli* Thioredoxin, *Biochemistry 36*, 15810−15816.
28. Ninfa, A. J., and Ballou, B. P. (1998) *Fundamental laboratory approaches for Biochemistry and Biotechnology*, pp 227−228, Fitzgerald Science Press, Bethesda, Maryland.
29. Hansen, R. E., Ostergaard, H., and Winther, J. R. (2005) Increasing the reactivity of an artificial dithiol-disulfide pair through modification of the electrostatic milieu, *Biochemistry 44*, 5899−5906.
30. Lennon, B. W., and Williams, C. H. (1996) Enzyme-monitored turnover of Escherichia coli thioredoxin reductase: Insights for catalysis, *Biochemistry 35*, 4704−4712.
31. Luthman, M., and Holmgren, A. (1982) Rat liver thioredoxin and thioredoxin reductase: purification and characterization, *Biochemistry 21*, 6628−6633.
32. Arscott, L. D., Thorpe, C., and Williams, C. H. (1981) Glutathione reductase from yeast. Differential reactivity of the nascent thiols in two-electron reduced enzyme and properties of a monoalkylated derivative, *Biochemistry 20*, 1513−1520.
33. Purich, D. L., and Allison, R. D. (1980) Isotope exchange methods for elucidating enzyme catalysis, *Methods Enzymol. 64*, 3−46.
34. Segel, I. (1975). *Enzyme Kinetics: Behavior and Analysis of Rapid Equilibrium and Steady-State Enzyme Systems*, pp 864−865, Wiley-Interscience, New York.
35. Moore, E. C., Reichard, P., and Thelander, L. (1964) Enzymatic synthesis of deoxyribonucleotides. V. Purification and properties of thioredoxin reductase from, *escherichia coli B. J. Biol. Chem. 239*, 3445−3452.
36. Krause, G., Lundstrom, J., Barea, J. L., Pueyo, de la Cuesta, C., and Holmgren, A. (1991) Mimicking the active site of protein disulfide-isomerase by substitution of proline 34 in Escherichia coli thioredoxin, *J. Biol. Chem. 266*, 9494−9500.
37. Clark, W. M. (1961) *Oxidation-reduction Potential of organic systems*, Williams and Wilkins, Baltimore.
38. Licht, S., Longo, K., Peramunage, D., and Forouzan, F. (1991) Conductometric analysis of the 2nd acid dissociation-constant of H_2S in highly concentrated aqueous-media, *J. Electroanal. Chem. 318*, 111−129.
39. Biterova, E. I., Turanov, A. A., Gladyshev, V. N., and Barycki, J. J. (2005) Crystal structures of oxidized and reduced mitochondrial thioredoxin reductase provide molecular details of the reaction mechanism, *Proc. Natl. Acad. Sci. U.S.A. 102*, 15018−15023.
40. Follmann, H., and Haberlein, I. (1996) Thioredoxins: universal, yet specific thiol-disulfide redox cofactors, *Biofactors 5*, 147−156.
41. Mora-Garcia, S., Rodriguez-Suarez, R., and Wolosiuk, R. A. (1998) Role of electrostatic interactions on the affinity of thioredoxin for target proteins. Recognition of chloroplast fructose-1, 6-bisphosphatase by mutant Escherichia coli thioredoxins, *J. Biol. Chem. 273*, 16273−16280.
42. Holmren, A. (1979) Reduction of disulfides by thioredoxin. Exceptional reactivity of insulin and suggested functions of thioredoxin in mechanism of hormone action, *J. Biol. Chem. 254*, 9113−9119.
43. Kallis, G. B., and Holmgren, A. (1980) Differential reactivity of the functional sulfhydryl groups of cysteine-32 and cysteine-35 present in the reduced form of thioredoxin from *Escherichia coli*. *J. Biol. Chem. 255*, 10261−10265.
44. Holmgren, A. (1995) Thioredoxin structure and mechanism: conformational changes on oxidation of the active-site sulfhydryls to a disulfide, *Structure 3*, 239−243.
45. Wahl, M. C., Irmler, A., Hecker, B., Schirmer, R. H., and Becker, K. (2005) Comparative structural analysis of oxidized and reduced thioredoxin from Drosophila melanogaster, *J. Mol. Biol. 345*, 1119−1130.

46. Arscott, L. D., Veine, D. M., and Williams, C. H. (2000) Mixed disulfide with glutathione as an intermediate in the reaction catalyzed by glutathione reductase from yeast and as a major form of the enzyme in the cell, *Biochemistry 39*, 4711−4721.
47. Houk, K. N., Leach, A. G., Kim, S. P., and Zhang, X. (2003) Binding affinities of host-guest, protein-ligand, and protein-transition-state complexes, *Angew. Chem., Int. Ed. 42*, 4872−4897.
48. Schmidt, H., and Krauth-Siegel, R. L. (2003) Functional and physicochemical characterization of the thioredoxin system in Trypanosoma brucei, *J. Biol. Chem. 278*, 46329−46336.
49. Cenas, N., Nivinskas, H., Anusevicius, Z., Sarlauskas, J., Lederer, F., and Arner, E. S. (2004) Interactions of quinones with thioredoxin reductase: a challenge to the antioxidant role of the mammalian selenoprotein, *J. Biol. Chem. 279*, 2583−2592.
50. Rakauskiene, G. A., Cenas, N. K., and Kulys, J. J. (1989) A "branched" mechanism of the reverse reaction of yeast glutathione reductase. An estimation of the enzyme standard potential values from the steady-state kinetics data, *FEBS Lett. 243*, 33−36.
51. Fersht, A., Ed.(1985) *Enzyme Structure and Mechanism*, 2nd ed., pp 105−106, WH Freeman and Company, New York.
52. Gromer, S., Arscott, L. D., Williams, C. H., Schirmer, R. H., and Becker, K. (1998) Human placenta thioredoxin reductase. Isolation of the selenoenzyme, steady state kinetics, and inhibition by therapeutic gold compounds, *J. Biol. Chem. 273*, 20096−20101.

BI700442R